The Journal of Chemical Physics

Calculation of electric quadrupole linestrengths for diatomic molecules: Application to the H_2, CO, HF, and O_2 molecules

Cite as: J. Chem. Phys. **155**, 214303 (2021); https://doi.org/10.1063/5.0063256
Submitted: 13 July 2021 • Accepted: 09 November 2021 • Accepted Manuscript Online: 10 November 2021 • Published Online: 01 December 2021

W. Somogyi, S. N. Yurchenko and A. Yachmenev

The Journal of Chemical Physics ARTICLE scitation.org/journal/jcp

Calculation of electric quadrupole linestrengths for diatomic molecules: Application to the H_2, CO, HF, and O_2 molecules

Cite as: J. Chem. Phys. 155, 214303 (2021); doi: 10.1063/5.0063256
Submitted: 13 July 2021 • Accepted: 9 November 2021 •
Published Online: 1 December 2021

W. Somogyi,[1,a] S. N. Yurchenko,[1,b] and A. Yachmenev[2,c]

AFFILIATIONS

[1] Department of Physics and Astronomy, University College London, Gower Street, WC1E 6BT London, United Kingdom
[2] Center for Free-Electron Laser Science CFEL, Deutsches Elektronen-Synchrotron DESY, Notkestraße 85, 22607 Hamburg, Germany and Center for Ultrafast Imaging, Universität Hamburg, Luruper Chaussee 149, 22761 Hamburg, Germany

[a] **Electronic mail:** wilfrid.somogyi.15@ucl.ac.uk
[b] **Author to whom correspondence should be addressed:** s.yurchenko@ucl.ac.uk
[c] **Electronic mail:** andrey.yachmenev@cfel.de

ABSTRACT

We present a unified variational treatment of the electric quadrupole (E2) matrix elements, Einstein coefficients, and linestrengths for general open-shell diatomic molecules in the general purpose diatomic code Duo. Transformation relations between the Cartesian representation (typically used in electronic structure calculations) to the tensorial representation (required for spectroscopic applications) of the electric quadrupole moment components are derived. The implementation has been validated against accurate theoretical calculations and experimental measurements of quadrupole intensities of $^1H_2$ available in the literature. We also present accurate electronic structure calculations of the electric quadrupole moment functions for the $X^1\Sigma^+$ electronic states of CO and HF, as well as for the $a^1\Delta_g$–$b^1\Sigma_g^+$ quadrupole transition moment of O_2 with the MRCI level of theory. Accurate infrared E2 line lists for $^{12}C^{16}O$ and $^1H^{19}F$ are provided. A demonstration of spectroscopic applications is presented by simulating E2 spectra for $^{12}C^{16}O$, $H^{19}F$, and $^{16}O_2$ (Noxon $a^1\Delta_g$–$b^1\Sigma_g^+$ band).

I. INTRODUCTION

The electric dipole approximation is often used to treat the spectra of diatomic, or small polyatomic, molecules. For most systems, this is a valid approximation that produces good results. For homonuclear diatomic molecules, however, electric dipole (E1) selection rules forbid pure rotational and vibrational transitions as well as parallel electronic transitions As a result, electric quadrupole (E2) transitions and magnetic dipole (M1) become important.[1–14]

This has implications for the spectra of several important molecules. The most famous example is the hydrogen molecule, which despite being the most abundant molecule in the universe has no infrared electric dipole spectrum. The three lowest lying electronic states of another important molecule, O_2, all have the same (*gerade*) symmetry, and transitions between them are therefore electric dipole forbidden.[5,15,16] Oxygen's significant absorption in the visible region comes from the electric quadrupole and magnetic dipole moments.

Even when electric dipole transitions are weakly allowed through interactions with other electronic states, E2 and M1 transitions may still be detectable, and their consideration is necessary for an accurate description of the molecule's spectrum,[17–20] such as for the Cameron bands ($a^3\Pi$–$X^1\Sigma$) and fourth positive system ($A^1\Pi$–$X^1\Sigma$) of CO.[18,21,22]

E2 and M1 transitions prove difficult to measure experimentally owing to their weak intensity and the long path lengths required for appreciable absorption. Electric quadrupole transition intensities are on the order of 10^6–10^9 times smaller than electric dipole transition intensities.[19,20,23] Nevertheless, they are often present in atmospheric spectra, where sufficiently long path lengths

are regularly achievable, and play an important role in geophysical and astrophysical applications.[3,5,22,24,25]

In spectroscopic applications as used in, e.g., the HITRAN database,[26] the E2 intensities are usually represented by expressions in terms of effective electric quadrupole moment constants with the rotational line intensities modeled via Hönl–London factors.[5,27] Examples of variational methodology used for electric quadrupole intensities of open-shell diatomic molecules include earlier works by Chiu;[28] Balasubramanian, D'Cunha, and Rao;[29] and Balasubramanian and Narayanan.[30]

Exoplanetary atmospheric retrievals require high resolution molecular opacities across a wide spectral range for a variety of temperatures. This has been the ongoing focus of the ExoMol database, and to date, molecular line lists have been produced for more than 80 molecules and 190 isotopologues.[31] However, several important homonuclear molecules, including N_2,[32] S_2, and the crucial biosignature molecule O_2,[33–37] have evaded rigorous treatment due to the dipole-forbidden nature of their spectra. As a result, these molecules are currently missing from analyses of atmospheric spectra of hot exoplanets, representing a significant obstacle to the characterization of exoplanet atmospheres or indeed any high temperature environments.

Here, we present a formulation of the electric quadrupole line intensities for a general (open-shell) diatomic molecule and an implementation of these E2 matrix element and linestrength expressions in the Duo program[38]—a powerful rovibronic variational program developed as part of the ExoMol project to solve the time-independent Schrödinger equations and compute rovibronic spectra of diatomics. To the best of our knowledge, this work represents the first general computational methodology for generating quadrupole spectra of arbitrary diatomic systems from first-principles, which lays the foundations for future work to produce a complete molecular line list for O_2 and other homonuclear diatomics.

This paper is structured as follows: Sec. II introduces the rovibronic basis used by the Duo program before presenting expressions for the electric quadrupole matrix elements, linestrengths, and Einstein coefficients for a general case of an arbitrary diatomic molecule. We also show how the matrix element components in the Cartesian representation, commonly employed in electronic structure calculations, are related to the tensorial representation used by Duo and outline the approach taken to reconstruct the transformation between the two. In Sec. III, we provide demonstrations for the Duo implementation of electric quadrupole linestrength calculations, including a validation against accurate theoretical and experimental linestrengths for H_2. We also present accurate quantum chemistry calculations of the electric quadrupole moment functions for CO and HF molecules, as well as infrared transition linestrengths for CO and HF molecules calculated using Duo. These line lists are included into the ExoMol database (www.exomol.com), which aims to provide molecular spectroscopic data for studies of exoplanetary and other atmospheres. More challenging nuclear motion applications of electronic E2 spectra of open-shell diatomic molecules are under way. As an illustration of an open-shell application, an E2 spectrum for the electronic system $a^1\Delta_g$–$b^1\Sigma_g^+$ (Noxon band) of O_2 is presented and compared to an experimental spectrum from the literature. The spectroscopic model for each molecule, including *ab initio* electric quadrupole moment functions $\Theta(r)$, is made available in the supplementary material via Duo input files. We also provide a list of calculated state energies and quantum numbers, as well as cross sections and line positions in the form of ExoMol line lists.[31]

II. THEORETICAL BACKGROUND

A. Matrix elements and linestrengths

1. Rovibronic wavefunctions

We consider the calculation of electric quadrupole spectra for an arbitrary diatomic molecule between some generic rovibronic states. Our aim is to implement an E2 spectra module as part of the general diatomic code Duo.[38] The original Duo program and its methodology are detailed extensively by Yurchenko *et al.*[38] For the purpose of defining the matrix elements here, it suffices to simply introduce the definition of the quadrupole moment, the basis functions, and the final eigenstates used by the Duo program. Duo uses Hund's case (a) basis set in the following form:

$$|\varphi_i\rangle = |\xi\Lambda\rangle|S\Sigma\rangle|\xi v\rangle|J\Omega M\rangle, \tag{1}$$

where J is the total angular momentum, M is a projection of J on the laboratory Z-axis in units of $\hbar$, S is the total electronic spin angular momentum, Σ is the projection of the spin of electrons on the molecular z-axis, ξ are indices of the ξth electronic state, Λ is the projection of the electronic angular momentum on the molecular z-axis, $\Omega = \Lambda + \Sigma$ (projection of the total angular momentum on the molecule z-axis), and v is the vibrational quantum number.

The eigenfunctions corresponding to the final rovibronic eigenvalues are expressed as linear combinations of the basis functions in Eq. (1),

$$|\psi_{JM\tau}\rangle = \sum_{\xi\Lambda S\Sigma v\Omega} C_{J\tau}(\xi\Lambda S\Sigma v\Omega)|\xi,\Lambda\rangle|S\Sigma\rangle|\xi,v\rangle|J\Omega M\rangle, \tag{2}$$

where $C_{J\tau}(\xi\Lambda S\Sigma v\Omega) = C_{J\tau}(\varphi)$ are the expansion coefficients obtained by solving a system of coupled rovibronic Schrödinger equations variationally and τ is the symmetry of a rovibronic eigenstate. In the case of a heteronuclear diatomic, τ is a parity $\tau = -$ (odd) or + (even),[39] which reflects how $|\psi_{JM\tau}\rangle$ transforms upon inversion or, equivalently, reflection through the molecule-fixed xz plane. For a homonuclear molecule, the symmetry τ includes the parity with respect to the permutation of the nuclei and is traditionally represented by the combinations ± (xz-reflection) as well as the g/u parities (molecular-fixed inversion), where g and u stand for "gerade" and "ungerade." Generally, the good quantum numbers are the total angular momentum J, the symmetry τ, and the g and u parities (homonuclear molecules). It is also common to assign other quantum numbers according to the largest coefficient $C_{J\tau}(\varphi)$ in the basis set expansion.[38]

2. Electric quadrupole matrix elements

The Einstein A coefficient for an E2 transition between a lower state i and an upper state f is given in SI units by

$$A_{fi} = \frac{8\pi^5\nu_{fi}^5}{5\varepsilon_0 hc^5}\frac{1}{(2J_f+1)}S_{fi}, \tag{3}$$

where ν_{fi} (s^{-1}) is the transition frequency, ε_0 (Fm^{-1}) is the permittivity of free space, h (J s) is Planck's constant, c (m s^{-1}) is the speed

of light in a vacuum,

$$S_{fi} = \left|M_{fi}^{(E2)}\right|^2 = \sum_{\alpha,\beta=x,y,z} \left|\langle \psi_f | Q_{\alpha\beta} | \psi_i \rangle\right|^2 \tag{4}$$

is the transition linestrength ($C^2\ m^4$), and the matrix elements are those of the quadrupole operator $Q_{\alpha\beta}$ ($\alpha, \beta = x, y$, or z) are defined relative to the nuclear center of mass by

$$Q_{\alpha\beta} = -\frac{3}{2}\sum_i e_i \left(r_{i,\alpha} r_{i,\beta} - \delta_{\alpha\beta}\frac{1}{3} r_i^2\right), \tag{5}$$

where the sum runs over the nuclei and electrons with e_i being the charge of the particle and r_i being its position vector in the molecule-fixed frame. We use the common convention of Buckingham,[40] used in many quantum chemistry programs such as in the work of Werner *et al.*[41] Different sources employ definitions of the quadrupole moment with varying constant pre-factors, such as Truhlar.[42]

The Duo rovibronic wavefunctions $|\psi_{JM\tau}\rangle$ and the transition linestrength in Eq. (4) are defined in the laboratory-fixed frame. Meanwhile, the electric quadrupole moments in Eq. (5) are defined in the molecule-fixed frame. For the convenience of calculating matrix elements, the relationship between the molecule-fixed and laboratory-fixed components of tensor operators is best established using the algebra of irreducible tensors. The traceless symmetric quadrupole tensor of rank 2 can be expressed in terms of three irreducible tensors $Q^{(0)}$, $Q^{(1)}$, and $Q^{(2)}$ with ranks zero, one, and two, respectively. The components $Q_m^{(k)}$ with $-k \le m \le k$ are expressed in terms of the Cartesian Q_{ij} via the following standard relations:[23,43]

$$Q_0^{(0)} = -\frac{1}{\sqrt{3}}(Q_{xx} + Q_{yy} + Q_{zz}), \tag{6}$$

$$Q_0^{(1)} = \frac{i}{\sqrt{2}}(Q_{xy} - Q_{yx}), \tag{7}$$

$$Q_{\pm1}^{(1)} = -\frac{1}{2}[Q_{xz} - Q_{zx} \pm i(Q_{zy} - Q_{yz})], \tag{8}$$

$$Q_0^{(2)} = \frac{1}{\sqrt{6}}(2Q_{zz} - Q_{xx} - Q_{yy}), \tag{9}$$

$$Q_{\pm1}^{(2)} = \frac{1}{2}[\mp(Q_{xz} + Q_{zx}) - i(Q_{yz} + Q_{zy})], \tag{10}$$

$$Q_{\pm2}^{(2)} = \frac{1}{2}[(Q_{xx} - Q_{yy}) \pm i(Q_{xy} + Q_{yx})] \tag{11}$$

and transform under rotation between the two frames as follows:[39]

$$Q_m^{(k)} = \sum_{m'} (-1)^{m-m'} Q_{m'}^{(k)} D_{-m,-m'}^{(k)}, \tag{12}$$

where $D_{-m,-m'}^{(k)}$ are the Wigner D-matrices. The traceless definition of the components $Q_{\alpha\beta}$ [Eq. (5)] and the property of being symmetric under interchange of the indices α, β imply that $Q_0^{(0)} = Q_m^{(1)} = 0$ such that only the second rank components of the quadrupole moment are non-zero. This allows one to write the transition linestrength using the Duo eigenfunctions [Eq. (2)] as

$$S_{fi} = g_{\rm ns} \sum_{M_i,M_f} \sum_{m=-2}^{2} \left|\left\langle \psi_{J_f M_f \tau_f} \middle| Q_m^{(2)} \middle| \psi_{J_i M_i \tau_i} \right\rangle\right|^2, \tag{13}$$

where $g_{\rm ns}$ is a nuclear statistical weight that accounts for the degenerate nuclear spin components of the total nuclear-rovibronic wavefunction (see, e.g., Bunker and Jensen).[44]

Long[43] provided expressions that allows one to construct laboratory frame matrix element expressions for the electric polarizability tensor—also of rank two. Adapting the treatment, one can write the transition quadrupole moment matrix elements as

$$\begin{aligned} S_{fi} = g_{\rm ns}(2J_i+1)(2J_f+1) &\left| \sum_{\varphi_f} C_{J_i\tau_i}^{*}(\varphi_f) \sum_{\varphi_i} C_{J_f\tau_f}(\varphi_i) \right. \\ &\times \sum_{m'} \delta_{S_f S_i} \delta_{\Sigma_f \Sigma_i} (-1)^{m'+\Omega_i} \langle v_f | \langle \xi_f \Lambda_f | Q_{m'}^{(2)} | \xi_i \Lambda_i \rangle | v_i \rangle \\ &\left. \times \begin{pmatrix} J_i & J_f & 2 \\ -\Omega_i & \Omega_f & -m' \end{pmatrix} \right|^2, \end{aligned} \tag{14}$$

where Eq. (12) was used to transform from the laboratory frame to the molecular frame. Here, m and m' index the components of the irreducible representation in the laboratory and molecular reference frames, respectively, and the following properties of the Wigner D-matrices, $D_{-m,-m'}^{(k)}$, have been used to express the rotational matrix element in terms of 3-j symbols,[39]

$$|JM\Omega\rangle = (-1)^{M-\Omega} \left(\frac{2J+1}{8\pi^2}\right)^{\frac{1}{2}} D_{-M,-\Omega}^{(J)}, \tag{15}$$

$$\langle JM\Omega| = \left(\frac{2J+1}{8\pi^2}\right)^{\frac{1}{2}} D_{M,\Omega}^{(J)}, \tag{16}$$

$$\int D_{cc'}^{C} D_{aa'}^{A} D_{bb'}^{B} \sin\beta \, d\beta \, d\alpha \, d\gamma = 8\pi^2 \begin{pmatrix} A & B & C \\ a & b & c \end{pmatrix} \begin{pmatrix} A & B & C \\ a' & b' & c' \end{pmatrix}, \tag{17}$$

with α, β, and γ being the Euler angles. Additionally, the following standard property of the 3-j symbols implies that the 3-j symbols containing $M_{\rm i}$, $M_{\rm f}$, and m, which arise as a result of Eq. (17), can be summed over $M_{\rm f}$, $M_{\rm i}$, and m and eliminated from Eq. (13),

$$\sum_{m=-k}^{k} \sum_{M'=-J'}^{J'} \sum_{M''=-J''}^{J''} \begin{pmatrix} J'' & k & J' \\ M'' & m & -M' \end{pmatrix}^2 = 1. \tag{18}$$

If required, e.g., for use with molecular dynamics programs such as RICHMOL,[45] Duo can explicitly calculate the laboratory frame components of the matrix elements. Note also that the 3-j symbols are invariant under cyclic permutations of their columns and have the properties $|A - B| \le C \le |A + B|$ and $a + b + c = 0$. Together with the

Kronecker deltas in Eq. (14), this implies the following selection rules for E2 transitions:

$$\Delta J = J_f - J_i = 0, \pm 1, \pm 2 \tag{19}$$

and $\Delta S = \Delta\Sigma = 0$ such that

$$\Delta\Lambda = \Lambda_f - \Lambda_i = -m = 0, \pm 1, \pm 2 \tag{20}$$

for all $\langle \xi_f \Lambda_f | Q_m^{(2)} | \xi_i \Lambda_i \rangle$ with $-2 \le m \le 2$ in Eq. (14). These quantum number selection rules should be supplemented by the symmetry selection rules,

$$+ \leftrightarrow +, \quad - \leftrightarrow -, \tag{21}$$

$$g \leftrightarrow g, \quad u \leftrightarrow u, \tag{22}$$

which arise as a result of the symmetric property of the quadrupole moment under coordinate inversion [Eq. (5)], and the requirement that the total matrix element is also symmetric under coordinate inversion such that the integral over spatial coordinates is non-zero.

3. Representation of ab initio coupling curves

In this section, we outline the procedure used by the Duo program to transform coupling curves, specifically including the independent components of the quadrupole moment tensor, from the Cartesian representation commonly obtained from electronic structure calculations to the tensorial, Λ-representation required by Duo. The (transition) quadrupole moments in Eq. (14) are r-dependent curves (r is the vibrational coordinate) averaged over electronic coordinates,

$$Q_m^{(2)}(r; \xi_f, \xi_i) = \langle \xi_f \Lambda_f | Q_m^{(2)}(r) | \xi_i \Lambda_i \rangle, \tag{23}$$

where $|\xi_i \Lambda_i\rangle$ and $|\xi_f \Lambda_f\rangle$ are the corresponding electronic wavefunctions. These curves are often obtained empirically by fitting analytical functions to experimental measurements of energies and linestrengths or computed *ab initio* using electronic structure programs such as those used in the present work (MOLPRO[41,46] or the open-access software CFOUR[47]). In electronic structure calculations, the representations of the infinite symmetry groups for diatomic molecules $C_{\infty v}$ and $D_{\infty h}$ are commonly represented in terms of their Abelian subgroups C_{2v} and D_{2h} in order to facilitate the computation of physically realized energy levels. For the practical purpose of transforming the electronic properties from the output of quantum chemistry programs to the representation required for the Duo input, we also employ the representation of $C_{\infty v}$ and $D_{\infty h}$ in terms of the Abelian subgroups in the following derivation.

The irreducible Abelian representation of a matrix element of a given operator coupling electronic states i and f, each with irreducible Abelian representations G_i and G_f, respectively, must be contained within the Abelian group given by the direct product $G_i \times G_f$.[23] Moreover, it can be shown that there exists only one independent Cartesian quadrupole component that couples a given pair of irreducible representations within an Abelian symmetry group. Tables I and II establish the correlations between the products of Cartesian vectors r_x, r_y, r_z, corresponding to the components of the quadrupole moment operator in Eq. (5), and the products of different irreducible representations for C_{2v} and D_{2h} point groups, respectively.

TABLE I. Product table for the quadratic functions of the Cartesian components and the isotropic function s, which transform as the product of different irreducible representations for the C_{2v} point group.

	A_1	A_2	B_1	B_2
A_1	s	xy	xz	yz
A_2	xy	s	yz	xz
B_1	xz	yz	s	xy
B_2	yz	xz	xy	s

Equation (14) uses the tensorial representation of all electronic properties, including the electric quadrupole moments $Q_m^{(2)}(r)$. It is also convenient to represent the electronic basis functions $|\xi\Lambda\rangle$ corresponding to the doubly degenerate $\Lambda > 0$ states in the tensorial representation with $\pm|\Lambda|$ as a good quantum number. These are related to the Cartesian components $|\alpha\rangle$ and $|\beta\rangle$ by[38]

$$|\xi, \pm|\Lambda|\rangle = \frac{1}{\sqrt{2}}[|\alpha\rangle \pm i|\beta\rangle], \tag{24}$$

where $|\alpha\rangle$ and $|\beta\rangle$ are, for example, $|\Pi_x\rangle$ and $|\Pi_y\rangle$ ($|\Lambda| = 1$), $|\Delta_{xx}\rangle$ and $|\Delta_{xy}\rangle$ ($|\Lambda| = 2$), etc., as typically produced by electronic structure methods.

We now consider the unitary transformation from the Cartesian (electronic structure) representation of the matrix elements $\langle \xi'' \gamma'' | Q_{ij}(r) | \xi' \gamma' \rangle$ ($\gamma \in [\alpha, \beta]$) to their tensorial (Duo) representation $\langle \xi'' \Lambda'' | Q_m^{(k)}(r) | \xi' \Lambda' \rangle$ in Eq. (23).

To construct this transformation and also to keep track of the relative phases of "electronic structure" wavefunctions, Duo makes the use of the Cartesian matrix elements of the electronic angular momentum operator $\hat{L}_z$. We choose the Cartesian components $|\alpha\rangle, |\beta\rangle$ such that for wavefunctions with $|\Lambda| > 0$ the $\hat{L}_z$ matrix is given (up to an arbitrary phase factor) by

$$\mathbf{L}_z = \begin{pmatrix} \langle\alpha|\hat{L}_z|\alpha\rangle & \langle\alpha|\hat{L}_z|\beta\rangle \\ \langle\beta|\hat{L}_z|\alpha\rangle & \langle\beta|\hat{L}_z|\beta\rangle \end{pmatrix} = \begin{pmatrix} 0 & -i\hbar|\Lambda| \\ i\hbar|\Lambda| & 0 \end{pmatrix}, \tag{25}$$

where $\mathbf{L}_z$ is the Cartesian matrix representation of $\hat{L}_z$ with the elements $\langle \xi\gamma'' | L_z | \xi\gamma' \rangle$ and the index ξ is dropped for simplicity. The wavefunctions $|\xi, \pm|\Lambda|\rangle$ in Eq. (24) can be formed as eigenfunctions

TABLE II. Product table for the quadratic functions of the Cartesian components and the isotropic function s, which transform as the product of different irreducible representations for the D_{2h} point group.

	A_g	B_{1g}	B_{2g}	B_{3g}	A_u	B_{1u}	B_{2u}	B_{3u}
A_g	s	xy	xz	yz				
B_{1g}	xy	s	yz	xz				
B_{2g}	xz	yz	s	xy				
B_{3g}	yz	xz	xy	s				
A_u					s	xy	xz	yz
B_{1u}					xy	s	yz	xz
B_{2u}					xz	yz	s	xy
B_{3u}					yz	xz	xy	s

of the operator $\hat{L}_z$ in the Cartesian representation by diagonalizing the 2×2 matrix $\mathbf{L}_z$ with the eigenvalues $\hbar|\Lambda|$ and $-\hbar|\Lambda|$.[38] The corresponding unitary matrix that diagonalizes $\mathbf{L}_z$,

$$U = \begin{pmatrix} \frac{1}{\sqrt{2}} & \frac{i}{\sqrt{2}} \\ \frac{1}{\sqrt{2}} & \frac{-i}{\sqrt{2}} \end{pmatrix}, \tag{26}$$

provides the transformation between the Cartesian and tensorial representations for any electronic structure property, including the electric quadrupole,

$$Q^{\text{tens.}} = U^{-1} Q^{\text{Cart.}} U. \tag{27}$$

Together with the 3-j symbol in Eq. (14), which implies that each component $Q^{(2)}_{m'}$ couples electronic states with $\Lambda_f - \Lambda_i = m'$, this allows for the following additional relations to be made:

$$\begin{aligned} \langle \pm|\Lambda||Q^{(2)}_0||\pm|\Lambda|\rangle &= \frac{3}{2\sqrt{6}}\left[\langle\alpha|Q_{zz}|\alpha\rangle + \langle\beta|Q_{zz}|\beta\rangle\right] \\ &= \frac{3}{\sqrt{6}}\langle\alpha|Q_{zz}|\alpha\rangle, \end{aligned} \tag{28}$$

$$\begin{aligned} \left\langle \Sigma^+\middle|Q^{(2)}_{\pm1}\middle|\mp\Pi\right\rangle &= \mp\frac{1}{\sqrt{2}}\left[\left\langle \Sigma^+\middle|Q_{xz}\middle|\Pi_x\right\rangle + \left\langle \Sigma^+\middle|Q_{yz}\middle|\Pi_y\right\rangle\right] \\ &= \mp\sqrt{2}\left\langle \Sigma^+\middle|Q_{xz}\middle|\Pi_x\right\rangle, \end{aligned} \tag{29}$$

$$\begin{aligned} \left\langle \Sigma^-\middle|Q^{(2)}_{\pm1}\middle|\mp\Pi\right\rangle &= -\frac{i}{\sqrt{2}}\left[\left\langle \Sigma^-\middle|Q_{xz}\middle|\Pi_y\right\rangle + \left\langle \Sigma^-\middle|Q_{yz}\middle|\Pi_x\right\rangle\right] \\ &= -i\sqrt{2}\left\langle \Sigma^-\middle|Q_{xz}\middle|\Pi_y\right\rangle, \end{aligned} \tag{30}$$

$$\begin{aligned} \left\langle \Sigma^+\middle|Q^{(2)}_{\pm2}\middle|\mp\Delta\right\rangle &= +\frac{1}{\sqrt{2}}\left[\left\langle \Sigma^+\middle|Q_{xx}\middle|\Delta_{xx}\right\rangle + \left\langle \Sigma^+\middle|Q_{xy}\middle|\Delta_{xy}\right\rangle\right] \\ &= +\sqrt{2}\left\langle \Sigma^+\middle|Q_{xx}\middle|\Delta_{xx}\right\rangle, \end{aligned} \tag{31}$$

$$\begin{aligned} \left\langle \Sigma^-\middle|Q^{(2)}_{\pm2}\middle|\mp\Delta\right\rangle &= \pm\frac{i}{\sqrt{2}}\left[\left\langle \Sigma^-\middle|Q_{xx}\middle|\Delta_{xy}\right\rangle + \left\langle \Sigma^-\middle|Q_{xy}\middle|\Delta_{xx}\right\rangle\right] \\ &= \pm i\sqrt{2}\left\langle \Sigma^-\middle|Q_{xx}\middle|\Delta_{xy}\right\rangle, \end{aligned} \tag{32}$$

$$\begin{aligned} \langle \mp\Pi|Q^{(2)}_{\pm1}|\mp\Delta\rangle &= \mp\frac{1}{2}\left[\langle\Pi_x|Q_{xz}|\Delta_{xx}\rangle + \langle\Pi_x|Q_{yz}|\Delta_{xy}\rangle\right. \\ &\quad \left. - \langle\Pi_y|Q_{yz}|\Delta_{xx}\rangle + \langle\Pi_y|Q_{xz}|\Delta_{xy}\rangle\right] \\ &= \mp 2\langle\Pi_x|Q_{xz}|\Delta_{xx}\rangle. \end{aligned} \tag{33}$$

The initial expressions in Eqs. (28)–(33) are obtained from Eqs. (9)–(11) by substituting the symmetric components $Q_{zx} = Q_{xz}$, $Q_{zx} = Q_{yz}$, $Q_{xy} = Q_{yx}$, and $Q_{xx} = -Q_{yy}$. The second line in each expression is obtained by setting the matrix elements that do not satisfy the selection rule in Eq. (20) (e.g., $\left\langle \Sigma^+\middle|Q^{(2)}_{\mp1}\middle|\mp\Pi\right\rangle$, $\left\langle \Sigma^+\middle|Q^{(2)}_{\mp2}\middle|\mp\Delta\right\rangle$, etc.) equal to zero and rearranging to obtain relations between different Cartesian components of the matrix elements. In the case of the D_{2h} symmetry, the corresponding equations [(28)–(33)] are identical except for the addition of the relevant g/u parity label.

III. DEMONSTRATIONS

In this section, we provide a demonstration of the Duo electric quadrupole program for the simple $^1\Sigma$ systems of H_2, CO, and HF. In particular, we choose H_2 as the initial proof of the program due to the highly accurate spectroscopic data available for this molecule, which we aim to reproduce. The demonstrations for CO and HF exemplify heteronuclear systems with large molecular quadrupole moments in which the consideration of E2 transitions is necessary to obtain accurate cross sections. An application to a more complex system involving interstate transitions with a non-Σ electronic state is illustrated by way of simulating the Noxon electronic (E2) band $a^1\Delta_g$–$b^1\Sigma^+_g$ of the O_2 molecule. The spectroscopic models detailed in this section are provided as supplementary material in the form of Duo input files, and the Duo program itself is open-source and can be obtained from the ExoMol public repository at github.com/Exomol.

A. Molecular hydrogen

Molecular hydrogen is the simplest diatomic molecule, containing just two electrons and two protons. It is the most abundant molecule in the universe and plays an important role in star formation,[48–51] interstellar physics,[52–54] (exo)planetary atmospheres,[55–58] and investigations of fundamental physics.[59,60]

Owing to its molecular symmetry, the homonuclear H_2 molecule has no permanent electric dipole moment, and thus, rovibrational transitions are forbidden in the electric dipole approximation. The availability of highly accurate electronic potential energy curves (PECs) and electric quadrupole moment curves (QMCs) makes H_2 an ideal candidate for validating the implementation of E2 transitions in Duo. The simplicity of the H_2 molecule makes it an extremely tractable quantum mechanical problem—indeed, it was the model molecule for many early calculations of molecular dynamics on the world's first mass-produced computers.[61–63] Even for these early calculations, linestrength accuracies within a few percent were attainable.[64–66] As a result, there is a wealth of accurate spectroscopic data available with which the Duo implementation can be validated. Most recently, Roueff *et al.*[12] calculated a highly accurate (order 10^{-6} cm^{-1}) infrared spectrum for the H_2 molecule including several higher order correction terms.[67]

The calculations of Roueff *et al.*[12] are based on an extensive series of earlier works by Pachucki[68] and Pachucki and Komasa,[69–71] in which the H_2 Born–Oppenheimer PEC was obtained with 10^{-15} relative numerical precision using 22 000 exponential basis functions and explicit electron correlation calculations.[68,72] They also compute non-adiabatic,[69,71] adiabatic,[70] and high-order relativistic[73] corrections to the Born–Oppenheimer potential energy. The quadrupole moment function employed in their calculations is obtained using the Born–Oppenheimer wavefunction and is in agreement with the values reported by Wolniewicz, Simbotin, and Dalgarno,[10] who employed a 494-term correlated basis representation of the wavefunction to obtain the quadrupole moment function with an estimated accuracy on the order of 0.001%.

For the validation of the Duo implementation, their original Born–Oppenheimer potential is retrieved using the V(DR) function made available via the H2SPECTRE program.[67] The contribution of the adiabatic and non-adiabatic corrections computed by Roueff *et al.*[12] is in the range of 5–20 and 0.4–4.0 cm^{-1},

respectively, increasing the total state energy. The higher order relativistic corrections are on the order of 0.01 cm^{-1} or less. Since the Born–Oppenheimer PEC provided does not include adiabatic or non-adiabatic corrections, significant deviation is expected between the calculated state energies for high v and J states. Typically, these deviations could be corrected in Duo via an empirical fit to experimentally accurate state energies. Such refinement is not performed in this work, as the aim here is to illustrate the implementation of E2 transition strengths rather than providing an accurate or improved line list for H_2. The quadrupole moment function of Wolniewicz, Simbotin, and Dalgarno[10] is also employed, given as a grid of 253 electric quadrupole moment values between 0.2 and 20.0 a_0, which Duo interpolates using quintic splines.

The vibrational grid is defined by 501 equally spaced points in the range of 0.38–18.90 a_0. After solving the vibrational Schrödinger equation using the sinc-DVR method, the first 30 vibrational states are selected to form the contracted vibrational basis and the rovibrational Schrödinger equation is solved for rotational states with total angular momentum quantum numbers $0 \le J \le 200$ at 296 K.

Figure 1 illustrates the results of a line-by-line comparison of the Duo results to the accurate line list of Roueff *et al.*[12] (including all corrections). As expected, significant differences between the energies calculated by Duo (E) and the accurate energies provided by H2SPECTRE ($\bar{E}$) for high v, J states are observed. We also expect to see a significant deviation in the Einstein coefficients obtained for transitions involving these states due to the factor of v_{fi}^5 present in Eq. (3) coupled with vanishingly small Einstein coefficients for transitions to states with a large v quantum number. Thus, states with $v \ge 10$ are excluded from the analysis.

For the 3027 remaining transitions between the remaining vibrational levels, 99.0% of the Einstein coefficients (A_{fi}) lie within 1% of the values calculated by Roueff *et al.*[12] ($\bar{A}_{fi}$). The 99th percentile is $|1 - A_{fi}/\bar{A}_{fi}| = 0.0672$. Note that all Einstein coefficients with errors greater than 5% correspond to weak transitions with absorption intensities $I_{fi} < 1 \times 10^{-35}$ cm molecule^{-1}. For example, the largest discrepancy $A_{fi}/\bar{A}_{fi} = 2.45$ corresponds to the $v = 9 \leftarrow 0$ transition with $A_{fi} = 5.27 \times 10^{-15}$ s^{-1} and $I_{fi} = 5.45 \times 10^{-36}$ cm molecule^{-1}.

Table III compares the results of the calculation to the experimentally measured intensities and line position of Bragg, Brault, and Smith[74] (T = 296 K) and Table IV to more recent measurements of

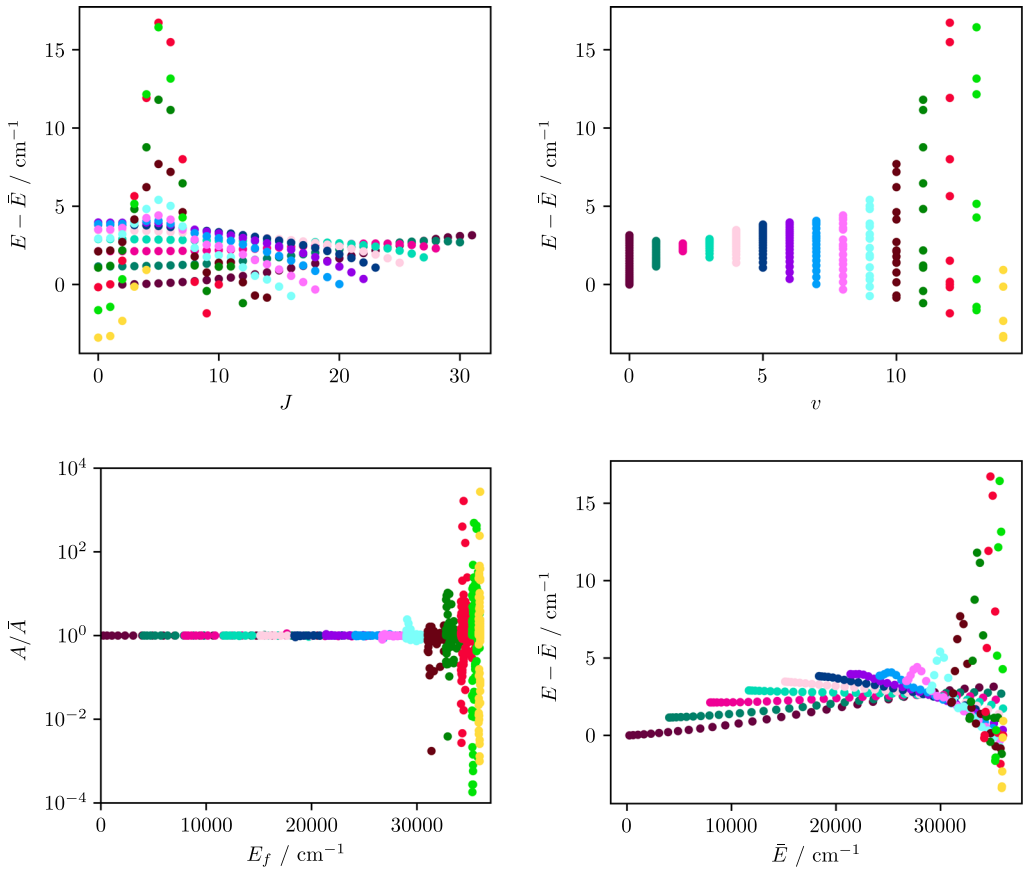

FIG. 1. Agreement between the Einstein A coefficients (bottom-left) and state energies of H_2 calculated by Duo (A_{if}, E) and by Roueff *et al.*[12] ($\bar{A}_{if}, \bar{E}$). The energy differences $E - \bar{E}$ in the upper panels are plotted as functions of the level of rotational J and vibrational v excitations. The energy and A-coefficient differences in the lower panels are plotted as functions of (upper) state energy. The colors in each plot correspond to the (upper) vibrational quantum number of the state.

TABLE III. Comparison of various H_2 $v' \leftarrow 0$ transitions (positions and intensities), measured experimentally by Bragg, Brault, and Smith[74] to the values predicted by Duo calculations at $T = 296$ K. The line positions are in cm^{-1}.

v'	Branch	$\tilde{\nu}_{obs.} - \tilde{\nu}^{Duo}_{calc.}$	$I_{obs.}/I^{Duo}_{calc.}$
1	Q(3)	−1.158	1.080
1	Q(2)	−1.165	1.027
1	Q(1)	−1.171	1.040
1	S(0)	−1.181	1.158
1	S(1)	−1.185	1.648
1	S(2)	−1.185	1.594
1	S(3)	−1.187	1.013
2	O(3)	−2.121	0.852
2	O(2)	−2.138	0.915
2	Q(3)	−2.121	0.949
2	Q(2)	−2.136	0.973
2	Q(1)	−2.147	1.624
2	S(0)	−2.152	0.984
2	S(1)	−2.147	0.988
3	S(0)	−2.923	0.816
3	S(1)	−2.912	0.911
3	S(2)	−2.887	1.017
3	S(3)	−2.858	0.878
4	S(0)	−3.480	0.606
4	S(1)	−3.469	0.874
4	S(2)	−3.432	0.727
4	S(3)	−3.382	0.831

Campargue *et al.*,[75] as well as their theoretical predictions based on the effective quadrupole moment method. The Duo calculated intensities reproduce closely the accurate experimental measurements of Campargue *et al.*[75] and match their theoretical predicted values to within 0.1%. Agreement with the older measurements of Bragg, Brault, and Smith[74] is less consistent but generally agrees, particularly for the *Q*-branch transitions of the first overtone band. In both cases, the line positions differ considerably, but by a roughly constant value across each vibrational band. This is due to the fact that no Duo refinement procedure is performed and no adiabatic or non-adiabatic corrections are included in the calculations. Also illustrated in Fig. 2 are (left) direct comparisons of the Einstein coefficients obtained via Duo to those of Roueff *et al.*[12] and (right) the absorption intensities via the EXOCROSS program, as compared to transitions listed in the HITRAN[26] database. Here and in the following, we use the HITRAN intensity units cm/molecule.

TABLE IV. Comparison of various H_2 $v' = 2 \leftarrow 0$ overtone lines, measured experimentally and computed via an effective quadrupole moment by Campargue *et al.*[75] ($\tilde{\nu}_{calc.}$), and the values predicted by Duo calculations ($\tilde{\nu}^{Duo}_{calc.}$) for $T = 296$ K. The line positions are in cm^{-1}.

Branch	$\tilde{\nu}_{obs.} - \tilde{\nu}_{calc.}$	$I_{obs.}/I_{calc.}$	$\tilde{\nu}_{obs.} - \tilde{\nu}^{Duo}_{calc.}$	$I_{obs.}/I^{Duo}_{calc.}$
O(5)	−0.0019	0.924	−2.061	0.924
O(4)	−0.0040	0.931	−2.093	0.930
O(3)	−0.0033	1.008	−2.115	1.007
O(2)	−0.0031	1.001	−2.132	1.000
O(5)	−0.0030	1.020	−2.067	1.020

B. Carbon monoxide

Carbon monoxide is a heteronuclear diatomic molecule, and thus, electric dipole transitions are allowed within its ground $X\ ^1\Sigma^+$ state. However, it also possesses a strong electric quadrupole moment,[77] and as a result, the electric dipole infrared spectrum is accompanied by weaker electric quadrupole lines. We show that many of the E2 spectral lines at room temperature lie higher in intensity than the minimum spectroscopic cutoff of 10^{-30} cm/molecule at the HITRAN reference temperature of $T = 296$ K, typically applied to E1 spectra. As a result, their inclusion or emission in spectroscopic databases has significant implications for applications where accurate cross sections are required.

Numerous experimental and *ab initio* studies have been performed for the electric dipole moment spectra of the CO molecule, including recent accurate calculations by Li *et al.*[78] Li *et al.* sought to resolve a long-standing uncertainty in the line intensities of CO E1 spectra, namely, significant differences observed between the intensities predicted by the calculations of Goorvitch[79] and those of Huré and Roueff.[80] The former used Chackerian's[81] semi-empirical dipole moment function, obtained from a nonlinear least-squares fit to vibrational states up to $v = 38$. The latter uses a purely *ab initio* electric dipole moment curve (DMC), computed by Langhoff and Bauschlicher via ACPF calculations on a 5Z basis set.[82] Li *et al.* performed new CRDS measurements in order to produce an accurate DMC via a direct fit. At long bond lengths, where experimental data are not attainable, they reproduce the calculations of Langhoff and Bauschlicher[82] but with a finer grid and determine that the interpolation used on the original grid was insufficient to capture the full shape of the DMC. Their PEC of choice is the analytical MLR3 function obtained by Coxon and Hajigeorgiou[83] via a direct fit to 21 559 spectroscopic lines.[83]

Studies of the quadrupole moment of CO are somewhat sparser. Although several experimental measurements exist for the equilibrium molecular quadrupole moment, only a single study presents a QMC across a range of geometries. The early work by Truhlar[42] presents simple Hartree–Fock calculations of the quadrupole moment at just six internuclear geometries. The accuracy of the vibrational matrix elements calculated is low, particularly for weaker transitions corresponding to higher vibrational quantum numbers. In particular, the methodology struggles to accurately describe the quadrupole moment at intermediate and long internuclear distances, which are necessary for calculating the vibrational overtones. Coriani *et al.*[84] compared the results of coupled-cluster single double (CCSD) and CC3 calculations on the CO molecule with a variety of basis sets. The results show that the CCSD level of theory is insufficient to correctly describe the electric properties of the CO molecule, and that the consideration of triple excitations is vital. They also studied the convergence of such calculations with increasing basis set size and found that the results converge quickly for bases larger than DZ.

In the present work, following the success of Coriani *et al.*,[84] the coupled-cluster single double triple [CCSD(T)] method is employed

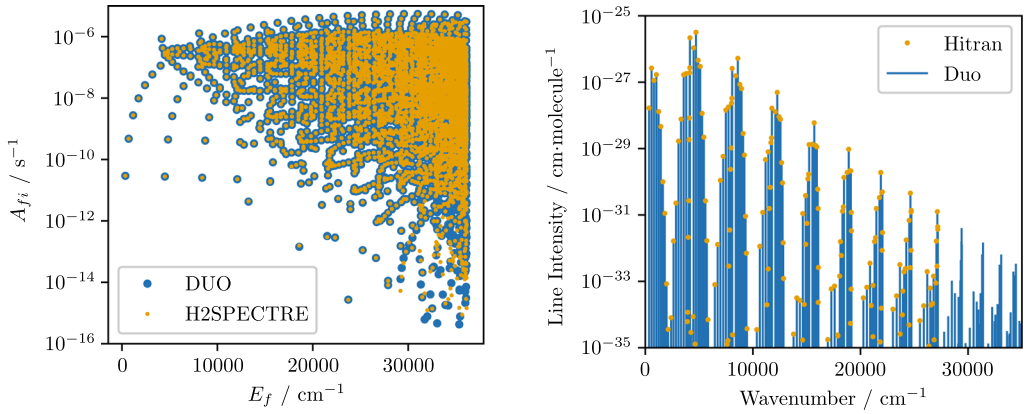

FIG. 2. Comparison of the Duo calculated Einstein *A* coefficients with the target values predicted by Roueff *et al.*[12] (left) and of the Duo calculated absorption intensities (T = 296 K) with the intensities listed in the HITRAN database[10,26,76] (right).

with an aug-cc-pwCVQZ basis as implemented in the CFOUR program[47] to calculate the strength of the non-zero quadrupole component Q_{zz} for 100 nuclear geometries in the range of 1.50–3.78 a_0. Divergent behavior at large internuclear separations is attributed to CCSD(T)'s inability to account for multireference effects. The curve is therefore truncated at 3.0 a_0. The QMC obtained from these calculations is shown in Fig. 3.

The value of the electric quadrupole moment curve at equilibrium separation Q_{zz} = −1.45 a.u. (a.u. = ea_0^2) agrees reasonably well with the Hartree–Fock calculations of Truhlar,[42] which obtain Q_{zz} = −1.33 a.u. Note that Truhlar[42] chose a definition of the quadrupole moment that is a factor of two larger than the definition employed by Molpro and Duo, and the value quoted here is adjusted accordingly. Importantly, we obtain very good agreement with experimental values of the ZPE-averaged quadrupole moment from the literature. From the CCSD(T) quadrupole moment shown in Fig. 3, Duo calculates $\langle v = 0|Q_{zz}|v = 0\rangle$ = −1.4522 a.u., which agrees closely

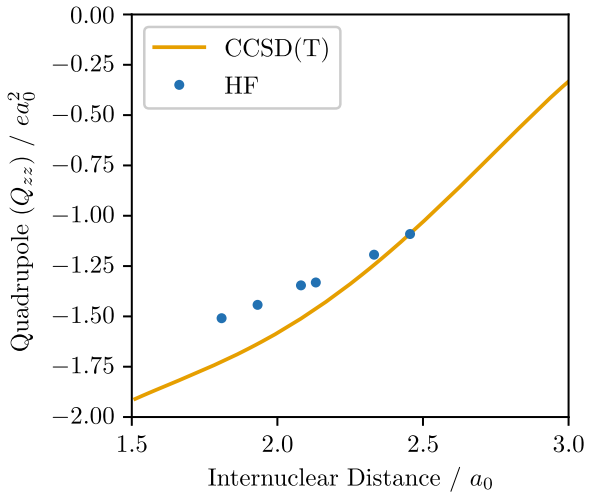

FIG. 3. Electric quadrupole moments in a.u. (ea_0^2) for CO obtained in this work via CCSD(T) calculations compared to Hartree–Fock calculations by Truhlar.[42]

with the accurate MBERS measurement of Meerts, Leeuw, and Dymanus;[85] the CC3 calculations of Coriani *et al.*;[84] and EFGIB measurements from other sources. These comparisons are presented in Table V.

Nuclear motion calculations are performed using the semi-empirical PEC of Meshkov *et al.*[89] This accurate analytical representation of the PEC is chosen for the Duo solutions in order to improve the quality of the wavefunctions used to calculate the linestrengths. The Duo vibrational grid used for the calculation consists of 501 equally spaced points in the range of 1.50–3.00 a_0, and the first 21 vibrational states are selected to form the contracted basis. These excitations correspond to energies within the spectroscopically relevant region (E/hc < 40.000 cm^{-1}) for the room temperature applications.

After solving the Schrödinger equation for rotational quantum numbers $0 \le J \le 50$, with a vibrational transition quadrupole moment, $\langle \xi_f v_f | Q_0^{(2)} | \xi_i v_i \rangle < 1 \times 10^{-5}$ a.u. are discarded. It was found by Medvedev *et al.*[90] that numerically computed transition dipole moments of high overtones corresponding to large changes in vibrational quanta can suffer from numerical instabilities and lead to unphysically large intensities. In the case of electric quadrupole

TABLE V. Comparison of various electric quadrupole moment values for CO in a.u. [ea_0^2 = 4.486 484(28) × 10^{-40} C m^2 [86]] from the literature. All values are averaged over the vibrational ZPE and are given in the molecular center of the mass reference frame, $Q_{zz}^{(CM)} = 2R_z\mu + Q_{zz}^{(EQC)}$ with the displacement between the center of mass and the electric quadrupole center given by R_z = −5.96 a.u. and a dipole moment of μ = −0.043 159 a.u.[77,84]

Q_{zz} (a.u.)	Method	References
−1.4522	CCSD(T)	This work
−1.445 (2)	CC3	84
−1.43 (3)	MBERS	85
−1.440 (69)	EFGIB	77
−1.382 (31)	EFGIB	77 and 87
−1.18 (22)	EFGIB	77 and 88

transitions, however, the intensity of these high overtone vibrational bands is sufficiently weak that absorption lines with transition quadrupole moments $\langle \xi_f v_f | Q_0^{(2)} | \xi_i v_i \rangle < 1 \times 10^{-5}$ a.u. (corresponding to high overtone bands) can simply be excluded from the line list altogether.

The calculated state energies are substituted for those obtained by Li *et al.*[78] in a simultaneous direct-fit to experimentally determined energy levels. This improves the accuracy in the line positions of the final stick spectrum, obtained via ExoCross,[91] but has no effect on the quadrupole Einstein coefficients or linestrengths. The energy level data of Li *et al.*[78] are made available through the HITRAN or ExoMol (exomol.com) databases.[31]

The resultant room temperature (T = 296 K) line list for $^{12}C^{16}O$ with a cutoff intensity of 10^{-35} cm molecule^{-1} consists of 6474 electric quadrupole transitions between rotational states up to J_{max} = 48 and vibrational states v = 7. A synthetic room temperature E2 spectrum is illustrated in Fig. 4, where it is compared to the E1 spectrum of Li *et al.*[78] The difference is approximately eight orders of magnitude. Nonetheless, many E2 lines—particularly for the $v = 0 \leftarrow 0$ and $v = 1 \leftarrow 0$ bands—lie above the typical cutoff intensity used in many spectroscopic databases (~10^{-30} cm^2 molecule^{-1} at T = 296 K).

The computed electric quadrupole Einstein A coefficients of $^{12}C^{16}O$ are combined with the ExoMol E1 line list Li2015 for CO in the form of an E2 transition file (see an extract in Table VI). Apart from the Einstein A E2 coefficients (s^{-1}), the transition file contains the upper and lower state counting numbers of the Li2015 state file, as illustrated in Table VII, which presents an extract from the ExoMol state file of the $^{12}C^{16}O$ line list Li2015. For more details on the ExoMol line list structure, see the work of Tennyson *et al.*[31]

TABLE VI. Extract from the $^{12}C^{16}O$ electric quadrupole transition file. It contains the upper (f) and lower (i) states counting numbers, Einstein A coefficients (s^{-1}), and transition wavenumbers (cm^{-1}).

f	i	A_{fi}	$\tilde{\nu}_{fi}$
94	10	1.0587×10^{-17}	10.591 935
93	9	1.1546×10^{-17}	10.696 876
92	8	1.2569×10^{-17}	10.801 832
91	7	1.3657×10^{-17}	10.906 802
90	6	1.4815×10^{-17}	11.011 786
89	5	1.6043×10^{-17}	11.116 781
88	4	1.7346×10^{-17}	11.221 787
87	3	1.8725×10^{-17}	11.326 802
86	2	2.0183×10^{-17}	11.431 825
85	1	2.1722×10^{-17}	11.536 856
136	52	1.7502×10^{-16}	17.652 735

C. Hydrogen fluoride

Like the CO molecule, HF possesses a strong permanent electric dipole moment,[93] and it also possesses a strong permanent electric quadrupole moment.[94] Numerous studies provide electronic structure calculations for properties of HF, including several which produce QMCs for the ground $X\ ^1\Sigma^+$ electronic state.[95–97] Piecuch *et al.*[95] used the orthogonally spin-adapted linear-response coupled-cluster (LRCC) theory with singly and doubly excited clusters (CCSD) and obtained quadrupole moments at 15 internuclear geometries in the range of 1.126 32–12.1296 a_0. Their basis set of choice is that introduced by Sadlej for correlated calculations of molecular electric properties,[98] which they compare to standard basis sets at the TZ level. They also provide the results of full CI calculations on a DZ basis set. Maroulis[96] presented all-electron CCSD(T) calculations of the quadrupole moment at nine internuclear geometries in the range of 0.9328–2.5328 a_0. For comparison, the quadrupole moment for the $X^1\Sigma^+$ state is computed via the multi-reference configuration interaction (MRCI) method and an aug-cc-pVQZ basis set at 501 internuclear geometries in the range of 1.32–6.99 a_0 using Molpro.

The electric quadrupole moments of HF obtained via these various methods are illustrated in Fig. 5. Although the four curves have the same general shape, significant variation is apparent between the value of Q_{zz} computed at intermediate bond lengths close to 3.8 a_0. Here, the strength of the quadrupole moment is greatest, and a difference of more than 0.5 a.u. is apparent between the full CI and CCSD methods. Table VIII shows the differences in the

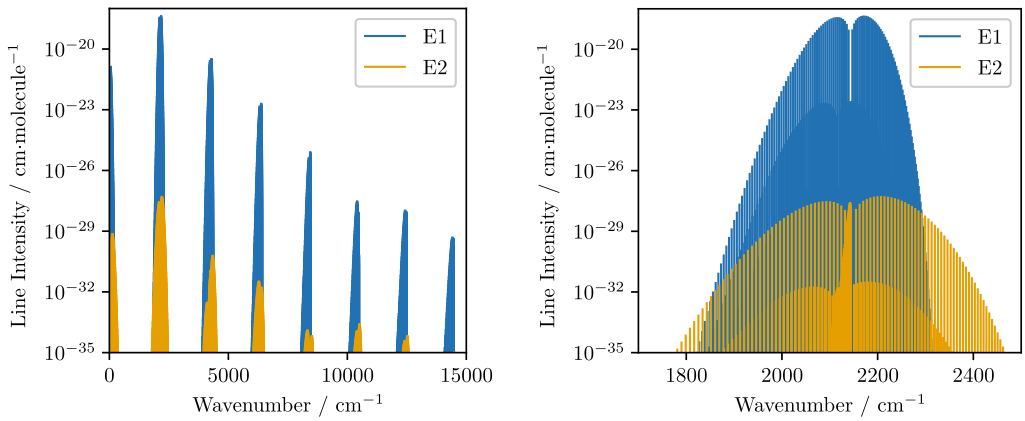

FIG. 4. Vibrational bands (left) and rotational v = 0–1 transitions (right) of the E1 and E2 rovibrational spectra in the ground $X\ ^1\Sigma^+$ state of the $^{12}C^{16}O$ molecule. The E1 intensities are those of Li *et al.*[78] via the ExoMol database.

TABLE VII. Extract from the Li2015 state file for $^{12}C^{16}O$. i: State counting number; $\tilde{E}$: state energy in cm^{-1}; g_i: total statistical weight, equal to $g_{ns}(2J+1)$; J: total angular momentum; v: state vibrational quantum number; and τ: rotationless parity e/f.[92]

i	E	g	J	v	τ
1	0.000 000	1	0	0	e
2	2 143.271 100	1	0	1	e
3	4 260.062 200	1	0	2	e
4	6 350.439 100	1	0	3	e
5	8 414.469 300	1	0	4	e
6	10 452.222 200	1	0	5	e
7	12 463.768 600	1	0	6	e
8	14 449.181 300	1	0	7	e
9	16 408.534 600	1	0	8	e
10	18 341.904 400	1	0	9	e
11	20 249.368 200	1	0	10	e

value of the quadrupole moment at the equilibrium internuclear distance for the four *ab initio* methods presented. All four calculations produce similar values for $Q_{zz}(R_e)$, but the coupled-cluster methods systematically overestimate the strength relative to experimental measurements. Importantly, when averaged over the vibrational ZPE, the MRCI results obtained in the present work give good agreement with the experimental MBERS measurement of de Leeuw and Dymanus.[94] They obtain $\langle v=0|Q_{zz}(r)|v=0\rangle = 1.75(2)$ a.u., while Duo calculates a value of 1.747 a.u., which is within the range of experimental uncertainties.

For the PEC, Coxon and Hajigeorgiou[99] provided a very accurate Rydberg–Klein–Rees (RKR)-style analytical expression for the potential energy and Born–Oppenheimer breakdown functions of the $X^1\Sigma^+$ ground electronic state of various hydrogen halide isotopologues, including $^1H^{19}F$. They devise a novel analytical form (MLR3) of the diatomic electronic potential and perform a nonlinear least-squares fit to experimental energies.

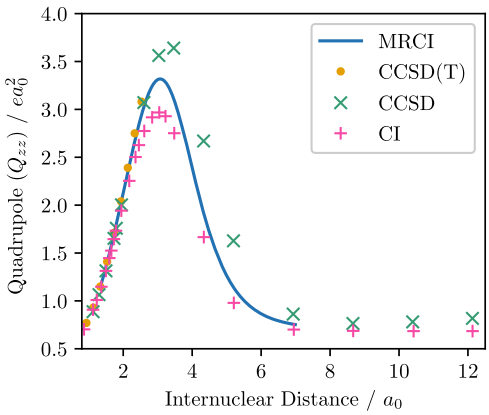

FIG. 5. Comparison of the quadrupole moment curves in a.u. (ea_0^2) for HF obtained via various *ab initio* methods. MRCI calculations presented in this work, CCSD(T) calculations of Maroulis,[96] and CCSD and full CI calculations of Piecuch *et al.*[95]

TABLE VIII. Comparison of various *ab initio* electric quadrupole moment values for HF in a.u. (ea_0^2). All values are given in the molecular center of the mass reference frame and at the equilibrium nuclear geometry.

Q_{zz} (a.u.)	Method	References
1.706	MRCI	This work
1.72	CCSD	95
1.72	CCSD(T)	96
1.66	CI	95

Their analytical representation of the MLR3 potential has been newly implemented in Duo, and for the present calculations, the HF MLR3 parameters obtained by Coxon and Hajigeorgiou[99] are employed, as well as their Born–Oppenheimer breakdown (BOB) function that is obtained from the Fortran source code provided in the supplementary material of Coxon and Hajigeorgiou.[99]

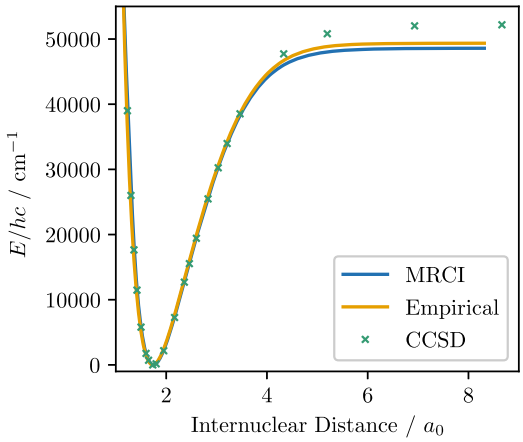

FIG. 6. Comparison of the potential energy curves for the $X^1\Sigma^+$ ground state of HF. MRCI calculations are from this work, empirically fitted MLR3 potential of Coxon and Hajigeorgiou,[99] and the CCSD calculations of Piecuch *et al.*[95]

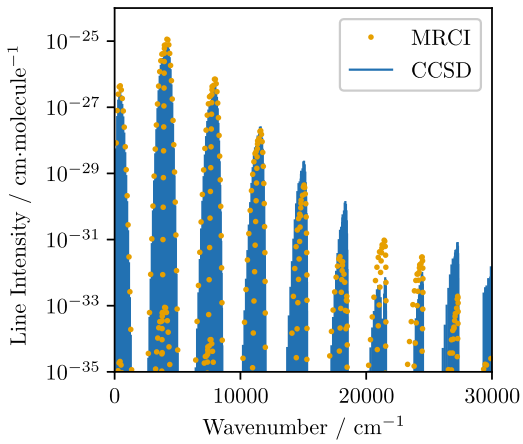

FIG. 7. Comparison of the electric quadrupole absorption spectrum for $H^{19}F$ obtained via spectroscopic models using the CCSD and MRCI quadrupole moment curves illustrated in Fig. 5.

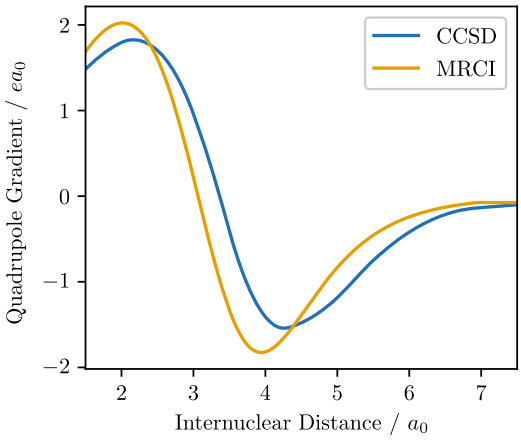

FIG. 8. Central finite difference gradients of the HF quadrupole moment obtained via MRCI and CCSD methods with respect to internuclear distance.

Figure 6 shows a comparison of the potential energy curves obtained from our MRCI calculations, the CCSD calculations of Piecuch *et al.*,[95] and the MLR3 potential of Coxon and Hajigeorgiou.[99] All three methods give similar results at short and intermediate bond lengths. The CCSD calculations overestimate the dissociation energy, relative to the empirical MLR3 potential, and the MRCI results predict a slightly lower dissociation energy. Figure 7 illustrates the results of calculations from two spectroscopic models. In each case, the potential energies are the same, the MLR3 and BOB curves of Coxon and Hajigeorgiou,[99] but one model uses the MRCI quadrupole moment presented in this work, and the other uses Piecuch's CCSD quadrupole moment. In both cases, nuclear motion calculations are performed for rotational states $0 \leq J \leq 41$, the vibrational grid is defined for 501 equally spaced points in the range of 0.76–4.40 a_0, and the first 20 vibrational states are chosen for the contracted basis.

For the first three vibrational bands, the absorption intensities predicted by both spectroscopic models are nearly identical. Higher order vibrational bands, however, exhibit significant discrepancies. The CCSD intensities begin to plateau above 20 000 cm^{-1}, and we propose that this intensity plateau arises as a result of the same effect encountered in Sec. III B and detailed by Medvedev *et al.*[90] Comparatively, the MRCI spectrum shows no such intensity plateau; indeed, the MRCI quadrupole moment is obtained on a considerably finer grid spacing, which aids in smoothing the interpolation.

A second possible cause proposed by Medvedev *et al.*[90] is the asymptotic behavior of the quadrupole moment curves at longer internuclear distances. Here, the magnitude of the coupling becomes exponentially smaller, and significant relative variations in the gradient of Q_{zz} are observed between the two methods. The gradient of the CCSD quadrupole moment curve at distances $R > 3\ a_0$ decays considerably slower than that obtained via MRCI calculations. Figure 8 shows the gradient of the two quadrupole moment functions computed using a central finite difference scheme on the Duo integration grid.

The MRCI spectrum exhibits a local minimum in intensity for the $v = 5 \leftarrow 0$ band. A similar abnormal intensity was observed by Medvedev *et al.*[90] for the same vibrational band of the electric dipole spectrum. Regardless, the expected E2 absorption intensities for the $v = 5 \leftarrow 0$ band are extremely weak, far weaker than typical spectroscopic cutoff intensity (10^{-30} cm/molecule at $T = 296$ K).

Intensities obtained using the MRCI quadrupole moment are chosen for the final $^1H^{19}F$ spectroscopic model and line list. This is combined with the ExoMol E1 line list Coxon–Hajigeorgiou in the form of an E2 transition file. Figure 9 compares the E2 intensities obtained for room temperature calculations to the E1 intensities of Coxon and Hajigeorgiou.[99] It consists of 2716 electric quadrupole transitions between rotational states up to $J = 18$ and vibrational states up to $v = 9$ with a cutoff intensity of 10^{-35} cm molecule^{-1} ($T = 296$ K) and is included into the supplementary material of this work.

D. Oxygen Noxon band

Owing to its molecular symmetry, the homonuclear O_2 molecule possesses no permanent dipole moment. Additionally,

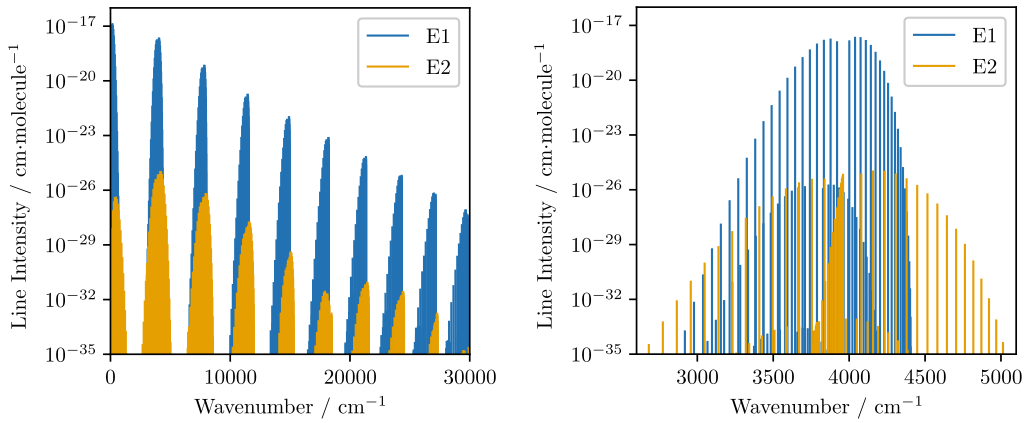

FIG. 9. Vibrational bands (left) and rotational $v = 0$–1 transitions (right) of the E1 and E2 rovibrational spectra in the ground $X^1\Sigma^+$ state of the $H^{19}F$ molecule as line intensities (cm/molecule). The E1 spectrum is that of Coxon and Hajigeorgiou,[99] via the ExoMol database.

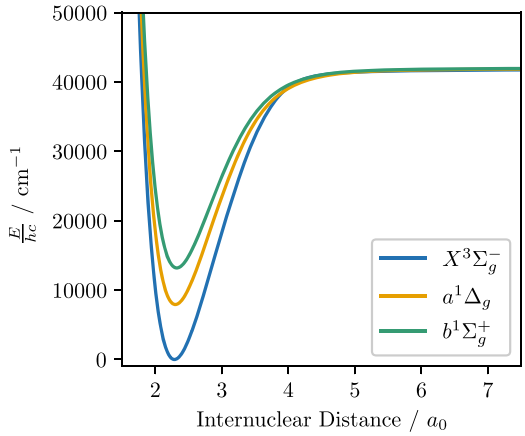

FIG. 10. Potential energy curves for the three lowest lying electronic states of O_2, obtained via MRCI calculations with an aug-cc-pV6Z basis set.

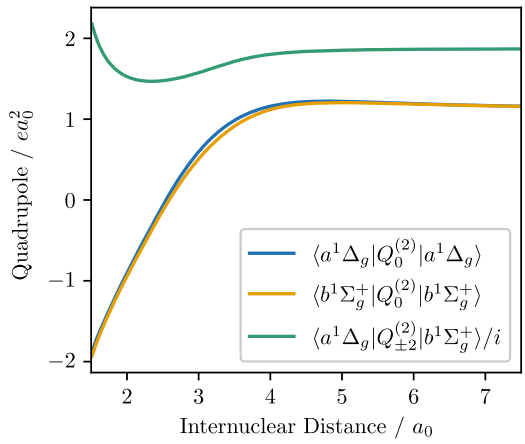

FIG. 11. Diagonal quadrupole moment curves in a.u. (ea_0^2) for the $a^1\Delta_g$ and $b^1\Sigma_g^+$ electronic states of O_2 obtained via MRCI calculations with an aug-cc-pV6Z basis set.

the three lowest lying electronic states, $X^3\Sigma_g^-$, $a^1\Delta_g$, and $b^1\Sigma_g^+$ all have *gerade* symmetry. The Σ spin–orbit mixing results in electric quadrupole transitions in the $a^1\Delta_g$–$X^3\Sigma_g^-$ system, which borrow strength from the direct $a^1\Delta_g$–$b^1\Sigma_g^+$ transitions of the so-called Noxon band,[27,100]

$$\langle a^1\Delta_g|Q_{\pm2}^{(2)}|X^3\Sigma_g^-\rangle \propto \langle a^1\Delta_g|Q_{\pm2}^{(2)}|b^1\Sigma_g^+\rangle. \tag{34}$$

Although weak, with the Einstein A coefficients on the order of 10^{-3} s^{-1}, rotational lines in both the (1–0) and (0–0) Noxon bands have been measured experimentally.[101,102] This electronic band is forbidden by the magnetic dipole $\Delta\Lambda = 0, \pm1$ selection rule, and consequently, the Noxon band is purely quadrupolar in nature. This makes the Noxon band ideal for validations of the electric quadrupole methodology applied to open-shell molecules.

The emission spectrum of the fundamental Noxon band was measured at 313(10) K by Fink *et al.*[102] with an estimated precision of 0.010–0.020 cm^{-1}. This measurement is replicated computationally with Duo calculated Einstein coefficients and the Exocross program. The *ab initio* data for the Duo calculations were produced using Molpro[103] with the MRCI program and an aug-cc-pV6Z basis set. The calculation includes PECs for the three lowest lying electronic states $X^3\Sigma_g^-$, $a^1\Delta_g$, and $b^1\Sigma_g^+$ (Fig. 10), as well as diagonal quadrupole moment curves $Q_0^{(2)}(r) = 3Q_{zz}(r)/\sqrt{6}$ for the $a^1\Delta_g$ and $b^1\Sigma_g^+$ electronic states, and the off-diagonal $a^1\Delta_g$–$b^1\Sigma_g^+$ quadrupole $Q_{\pm2}^{(2)}(r) = \sqrt{2}Q_{xx}(r)$ (Fig. 11). The calculations are performed on a grid of 116 internuclear distances in the range of 1.5–7.5 a_0. The contracted vibrational basis set consists of the first 25 vibrational states for each electronic state, and the calculations are performed for rotational states $0 \le J \le 50$.

Figure 12 shows an overlay of the experimental spectrum by Fink *et al.*[102] with the calculated emission cross section for the fundamental Noxon band, obtained via Exocross using the Duo calculated Einstein coefficients at 313 K with a Voigt line profile (HWHM = 0.15 cm^{-1}). The intensities have been scaled relative to the most intense $Q(8)$ transition. There is a systematic error in the line positions calculated by Duo ~7 cm^{-1}, which is attributed primarily to the fact that the calculations do not include the strongly coupled excited $C^3\Pi_g$ state.[30] Due to the number of couplings required for a complete treatment of the open-shell O_2 molecule, the full rovibronic spectrum including such highly excited states will be the focus of a future publication. Consequently, and for the sake of simplicity, no empirical refinement of the PECs is performed in the present work. Nonetheless, the relative line positions and intensities are in good agreement with those measured by Fink *et al.*[102] and demonstrate the validity of the approach for open-shell diatomic systems and excited electronic states.

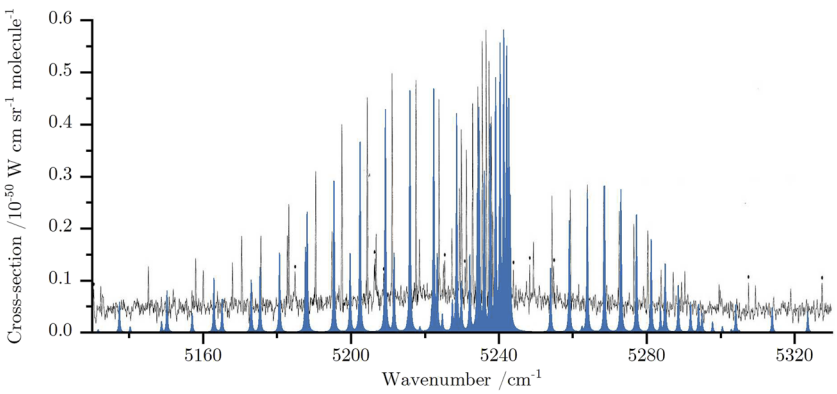

FIG. 12. Overlay of the Duo calculated O_2 Noxon emission cross sections with the measured spectrum from Fink *et al.*,[102] scaled relative to the peak intensity of the $Q(8)$ transition. The cross sections are calculated at T = 313 K with a Voigt profile (HWHM = 0.15 cm^{-1}).

IV. CONCLUSIONS

Generic expressions for the electric quadrupole Einstein coefficients and matrix elements between arbitrary electronic states of (open-shell) diatomic molecules have been derived and implemented in the Duo spectroscopic code. The implementation is general and allows for the creation of highly accurate *ab initio* and empirical spectroscopic models and line lists for an array of astrophysically important molecules. This work has been validated by reproducing highly accurate literature data for the homonuclear H_2 molecule as well as by comparison to the electronic emission spectrum of the O_2 Noxon band, and further demonstrated by the calculation of novel electric quadrupole spectra for the heteronuclear CO and HF molecules. The line lists for CO and HF have been included in the ExoMol database.

Through this calculation, we have shown that even for electric dipole-allowed systems, electric quadrupole line intensities can often lie above the typically cutoff intensities used in spectroscopic databases, atmospheric retrievals, and remote-sensing applications. For many homonuclear systems where rovibrational, and many electronic, transitions are forbidden in the electric dipole approximation, the calculation of the quadrupole intensities is crucial for producing accurate rovibronic line lists. Our goal is to provide accurate E2 and M1 line lists for electronic transitions of (open-shell) diatomic molecules such as O_2, N_2, S_2, and SO.

SUPPLEMENTARY MATERIAL

See the supplementary material for the spectroscopic models for H_2, HF, CO, and O_2 in the form of Duo input files; E2 line lists for H_2, HF, CO, and O_2 using the ExoMol format; and examples of E2 room temperature spectra of these molecules with the upper and lower states fully assigned.

ACKNOWLEDGMENTS

This work was supported by STFC Project Nos. ST/R000476/1 and ST/S506497/1. The authors acknowledge the use of the UCL Legion High Performance Computing Facility (Myriad@UCL) and associated support services in the completion of this work. This work was also supported by the European Research Council (ERC) under the European Union's Horizon 2020 research and innovation program through Advance Grant No. 883830. The work of A.Y. was supported by the Deutsches Elektronen-Synchrotron (DESY), a member of the Helmholtz Association (HGF), and by the Deutsche Forschungsgemeinschaft (DFG) through the cluster of excellence "Advanced Imaging of Matter" (AIM, EXC 2056, ID 390715994).

AUTHOR DECLARATIONS

Conflict of Interest

The authors have no conflicts to disclose.

DATA AVAILABILITY

The data that support the findings of this study are available within the article and its supplementary material and are also openly available at www.exomol.com.

APPENDIX: CORRELATION OF MOLPRO ENUMERATION TO TERM SYMBOLS

Tables XI and XII are versions of Tables IX and X with the addition of Molpro enumerations for the irreducible representations, which can be used to simplify the conversion of Molpro output data into Duo input.

TABLE IX. Irreducible representations for homonuclear symmetry groups and corresponding components of electronic states. The Appendix gives the same table with the addition of the Molpro enumerations.

Symmetry	Components
A_g	Σ_g^+, $(\Delta_g)_{xx}$
B_{1g}	Σ_g^-, $(\Delta_g)_{xy}$
B_{2g}	$(\Pi_g)_x$
B_{3g}	$(\Pi_g)_y$
A_u	Σ_u^-, $(\Delta_u)_{xy}$
B_{1u}	Σ_u^+, $(\Delta_u)_{xx}$
B_{2u}	$(\Pi_u)_y$
B_{3u}	$(\Pi_u)_x$

TABLE X. Irreducible representations for heteronuclear symmetry groups and corresponding components of electronic states. The Appendix gives the same table with the addition of the Molpro enumerations.

Symmetry	Components
A_1	Σ^+, Δ_{xx}
A_2	Σ^-, Δ_{xy}
B_1	Π_x
B_2	Π_y

TABLE XI. Irreducible representations for homonuclear symmetry groups, the functions that transform according to the irreducible representations, their Molpro enumeration, and corresponding components of electronic states.

Symmetry	Function	molpro No.	Components
A_g	s	1	Σ_g^+, $(\Delta_g)_{xx}$
B_{1g}	xy	4	Σ_g^-, $(\Delta_g)_{xy}$
B_{2g}	xz	6	$(\Pi_g)_x$
B_{3g}	yz	7	$(\Pi_g)_y$
A_u	xyz	8	Σ_u^-, $(\Delta_u)_{xy}$
B_{1u}	z	5	Σ_u^+, $(\Delta_u)_{xx}$
B_{2u}	y	3	$(\Pi_u)_y$
B_{3u}	x	2	$(\Pi_u)_x$

TABLE XII. Irreducible representations for heteronuclear symmetry groups, the functions that transform according to the irreducible representations, their Molpro enumeration, and corresponding components of electronic states.

Symmetry	Function(s)	molpro No.	Components
A_1	s, z	1	Σ^+, Δ_{xx}
A_2	xy	4	Σ^-, Δ_{xy}
B_1	x, xz	2	Π_x
B_2	y, yz	3	Π_y

REFERENCES

[1] J. Reid, R. L. Sinclair, A. M. Robinson, and A. R. W. McKellar, Phys. Rev. A **24**, 1944 (1981).
[2] J. W. Brault, J. Mol. Spectrosc. **80**, 384 (1980).
[3] A. Goldman, J. Reid, and L. S. Rothman, Geophys. Res. Lett. **8**, 77, https://doi.org/10.1029/gl008i001p00077 (1981).
[4] L. S. Rothman and A. Goldman, Appl. Opt. **20**, 2182 (1981).
[5] I. E. Gordon, S. Kassi, A. Campargue, and G. C. Toon, J. Quant. Spectrosc. Radiat. Transfer **111**, 1174 (2010).
[6] O. Leshchishina, S. Kassi, I. E. Gordon, S. Yu, and A. Campargue, J. Quant. Spectrosc. Radiat. Transfer **112**, 1257 (2011).
[7] D. Reuter, D. E. Jennings, and J. W. Brault, J. Mol. Spectrosc. **115**, 294 (1986).
[8] P. Čermák, S. Vasilchenko, D. Mondelain, S. Kassi, and A. Campargue, Chem. Phys. Lett. **668**, 90 (2017).
[9] G. Herzberg, Nature **163**, 170 (1949).
[10] L. Wolniewicz, I. Simbotin, and A. Dalgarno, Astrophys. J., Suppl. Ser. **115**, 293 (1998).
[11] S.-M. Hu, H. Pan, C.-F. Cheng, Y. R. Sun, X.-F. Li, J. Wang, A. Campargue, and A.-W. Liu, Astrophys. J. **749**, 76 (2012).
[12] E. Roueff, H. Abgrall, P. Czachorowski, K. Pachucki, M. Puchalski, and J. Komasa, Astron. Astrophys. **630**, A58 (2019).
[13] K. D. Setzer, M. Kalb, and E. H. Fink, J. Mol. Spectrosc. **221**, 127 (2003).
[14] L. Augustovičová, W. P. Kraemer, V. Špirko, and P. Soldán, Mon. Not. R. Astron. Soc. **446**, 2738 (2014).
[15] H. Liu, D. Shi, J. Sun, Z. Zhu, and Z. Shulin, Spectrochim. Acta, Part A **124**, 216 (2014).
[16] S. Yu, C. E. Miller, B. J. Drouin, and H. S. P. Müller, J. Chem. Phys. **137**, 024304 (2012).
[17] S. G. Tilford and J. D. Simmons, J. Chem. Phys. **44**, 4145 (1966).
[18] S. G. Tilford and J. D. Simmons, J. Phys. Chem. Ref. Data **1**, 147 (1972).
[19] A. Campargue, S. Kassi, A. Yachmenev, A. A. Kyuberis, J. Küpper, and S. N. Yurchenko, Phys. Rev. Res. **2**, 023091 (2020).
[20] A. Campargue, A. M. Solodov, A. A. Solodov, A. Yachmenev, and S. N. Yurchenko, Phys. Chem. Chem. Phys. **22**, 12476 (2020).
[21] P. H. Krupenie, *The Band Spectrum of Carbon Monoxide* (U.S. Department of Commerce, National Bureau of Standards, 1966).
[22] R. J. Glinski, J. A. Nuth, M. D. Reese, and M. L. Sitko, Astrophys. J. **467**, L109 (1996).
[23] P. R. Bunker and P. Jensen, *Molecular Symmetry and Spectroscopy*, 2nd ed. (NRC Research Press, Ottawa, Canada, 2006).
[24] A. Goldman, C. P. Rinsland, B. Canova, R. Zander, and M. Dang-Nhu, J. Quant. Spectrosc. Radiat. Transfer **54**, 757 (1995).
[25] J. Domysławska, S. Wójtewicz, P. Masłowski, A. Cygan, K. Bielska, R. S. Trawiński, R. Ciuryło, and D. Lisak, J. Quant. Spectrosc. Radiat. Transfer **169**, 111 (2016).
[26] I. E. Gordon *et al.*, J. Quant. Spectrosc. Radiat. Transfer **203**, 3 (2017).
[27] A. P. Mishra, T. K. Balasubramanian, and B. J. Shetty, J. Quant. Spectrosc. Radiat. Transfer **112**, 2303 (2011).
[28] Y.-N. Chiu, J. Chem. Phys. **42**, 2671 (1965).
[29] T. K. Balasubramanian, R. D'Cunha, and K. N. Rao, J. Mol. Spectrosc. **144**, 374 (1990).
[30] T. K. Balasubramanian and O. Narayanan, Acta Phys. Hung. **74**, 341 (1994).
[31] J. Tennyson, S. N. Yurchenko, A. F. Al-Refaie, V. H. J. Clark, K. L. Chubb, E. K. Conway, A. Dewan, M. N. Gorman, C. Hill, A. E. Lynas-Gray, T. Mellor, L. K. McKemmish, A. Owens, O. L. Polyansky, M. Semenov, W. Somogyi, G. Tinetti, A. Upadhyay, I. Waldmann, Y. Wang, S. Wright, and O. P. Yurchenko, J. Quant. Spectrosc. Radiat. Transfer **255**, 107228 (2020).
[32] H. Lammer, L. Sproß, J. L. Grenfell, M. Scherf, L. Fossati, M. Lendl, and P. E. Cubillos, Astrobiology **19**, 927 (2019).
[33] V. S. Meadows, C. T. Reinhard, G. N. Arney, M. N. Parenteau, E. W. Schwieterman, S. D. Domagal-Goldman, A. P. Lincowski, K. R. Stapelfeldt, H. Rauer, S. DasSarma, S. Hegde, N. Narita, R. Deitrick, J. Lustig-Yaeger, T. W. Lyons, N. Siegler, and J. L. Grenfell, Astrobiology **18**, 630 (2018).
[34] A. E. Doyle, E. D. Young, B. Klein, B. Zuckerman, and H. E. Schlichting, Science **366**, 356 (2019).
[35] L. Schaefer, R. D. Wordsworth, Z. Berta-Thompson, and D. Sasselov, Astrophys. J. **829**, 63 (2016).
[36] E. S. Kite and L. Schaefer, Astrophys. J., Lett. **909**, L22 (2021).
[37] C. M. Lisse, S. J. Desch, C. T. Unterborn, S. R. Kane, P. R. Young, H. E. Hartnett, N. R. Hinkel, S.-H. Shim, E. E. Mamajek, and N. R. Izenberg, Astrophys. J. **898**, L17 (2020).
[38] S. N. Yurchenko, L. Lodi, J. Tennyson, and A. V. Stolyarov, Comput. Phys. Commun. **202**, 262 (2016).
[39] H. Kato, Bull. Chem. Soc. Jpn. **66**, 3203 (1993).
[40] A. D. Buckingham, Q. Rev. (London, Engl.) **13**, 183 (1959).
[41] H.-J. Werner, P. J. Knowles, G. Knizia, F. R. Manby, and M. Schütz, Wiley Interdiscip. Rev.: Comput. Mol. Sci. **2**, 242 (2012).
[42] D. G. Truhlar, Int. J. Quantum Chem. **6**, 975 (1972).
[43] D. A. Long, *The Raman Effect: A Unified Treatment of the Theory of Raman Scattering by Molecules* (Wiley, Chichester, New York, 2002).
[44] P. Jensen and P. R. Bunker, Fundamentals of molecular symmetry, 1st ed. (Institute of Physics, 2005).
[45] A. Yachmenev, L. V. Thesing, and J. Küpper, J. Chem. Phys. **151**, 244118 (2019).
[46] H.-J. Werner, P. J. Knowles, F. R. Manby, J. A. Black, K. Doll, A. Heßelmann, D. Kats, A. Köhn, T. Korona, D. A. Kreplin, Q. Ma, T. F. Miller, A. Mitrushchenkov, K. A. Peterson, I. Polyak, G. Rauhut, and M. Sibaev, J. Chem. Phys. **152**, 144107 (2020).
[47] J. Stanton, J. Gauss, M. Harding *et al.*, cFOUR, a quantum chemical program package written by J. F. Stanton, J. Gauss, M. E. Harding, and P. G. Szalay with contributions from A. A. Auer, R. J. Bartlett, U. Benedikt, C. Berger, D. E. Bernholdt, Y. J. Bomble, L. Cheng, O. Christiansen, M. Heckert, O. Heun, C. Huber, T.-C. Jagau, D. Jonsson, J. Jusélius, K. Klein, W. J. Lauderdale, D. A. Matthews, T. Metzroth, L. A. Mück, D. P. O'Neill, D. R. Price, E. Prochnow, C. Puzzarini, K. Ruud, F. Schiffmann, W. Schwalbach, S. Stopkowicz, A. Tajti, J. Vázquez, F. Wang, and J. D. Watts and the integral packages MOLECULE (J. Almlöf and P. R. Taylor), PROPS (P. R. Taylor), ABACUS (T. Helgaker, H. J. Aa. Jensen, P. Jørgensen, and J. Olsen), and ECP routines by A. V. Mitin and C. van Wüllen. For the current version, see http://www.cfour.de, 2019.
[48] H. R. Johnson, J. H. Goebel, D. Goorvitch, and S. T. Ridgway, Astrophys. J., Lett. **270**, L63 (1983).
[49] H. J. Fraser, M. R. S. McCoustra, and D. A. Williams, Astron. Geophys. **43**, 2–10 (2002).
[50] H. Kreckel, H. Bruhns, M. Čížek, S. C. O. Glover, K. A. Miller, X. Urbain, and D. W. Savin, Science **329**, 69 (2010).
[51] B. Nisini, T. Giannini, D. A. Neufeld, Y. Yuan, S. Antoniucci, E. A. Bergin, and G. J. Melnick, Astrophys. J. **724**, 69 (2010).
[52] F. Islam, C. Cecchi-Pestellini, S. Viti, and S. Casu, Astrophys. J. **725**, 1111 (2010).
[53] D. J. Hollenbach and A. G. G. M. Tielens, Rev. Mod. Phys. **71**, 173 (1999).
[54] A. Dalgarno, in *Molecular Hydrogen in Space*, Cambridge Contemporary Astrophysics, edited by F. Combes and G. DesForets (PCMI-CNRS; Collaborat Computat Project 7; Observ Paris; Minist Affaires Etrangeres; Univ Cergy Pontoise; Univ Paris XI; Inst Astrophys Paris, 2000), pp. 3–11.
[55] B. P. Bowler, M. C. Liu, T. J. Dupuy, and M. C. Cushing, Astrophys. J. **723**, 850 (2010).
[56] C. M. Huitson, D. K. Sing, A. Vidal-Madjar, G. E. Ballester, A. L. des Etangs, J.-M. Désert, and F. Pont, Mon. Not. R. Astron. Soc. **422**, 2477 (2012).
[57] K. B. Stevenson, J. L. Bean, A. Seifahrt, J.-M. Désert, N. Madhusudhan, M. Bergmann, L. Kreidberg, and D. Homeier, Astrophys. J. **147**, 161 (2014).
[58] A. Ardaseva, P. B. Rimmer, I. Waldmann, M. Rocchetto, S. N. Yurchenko, C. Helling, and J. Tennyson, Mon. Not. R. Astron. Soc. **470**, 187 (2017).
[59] W. Ubachs, J. C. J. Koelemeij, K. S. E. Eikema, and E. J. Salumbides, J. Mol. Spectrosc. **320**, 1 (2016).
[60] W. Ubachs, J. Bagdonaite, E. J. Salumbides, M. T. Murphy, and L. Kaper, Rev. Mod. Phys. **88**, 021003 (2016).
[61] W. Kolos and L. Wolniewicz, Rev. Mod. Phys. **35**, 473 (1963).

[62]W. Kolos and L. Wolniewicz, J. Chem. Phys. **43**, 2429 (1965).
[63]R. J. LeRoy and R. B. Bernstein, J. Chem. Phys. **49**, 4312 (1968).
[64]A. DalGarno, A. C. Allison, and J. C. Browne, J. Atmos. Sci. **26**, 946 (1969).
[65]G. Karl and J. D. Poll, J. Chem. Phys. **46**, 2944–2950 (1967).
[66]J. Turner, K. Kirby-Docken, and A. Dalgarno, Astrophys. J., Suppl. Ser. **35**, 281 (1977).
[67]J. Komasa, M. Puchalski, P. Czachorowski, G. Łach, and K. Pachucki, Phys. Rev. A **100**, 032519 (2019).
[68]K. Pachucki, Phys. Rev. A **82**, 032509 (2010).
[69]K. Pachucki and J. Komasa, J. Chem. Phys. **130**, 164113 (2009).
[70]K. Pachucki and J. Komasa, J. Chem. Phys. **141**, 224103 (2014).
[71]K. Pachucki and J. Komasa, J. Chem. Phys. **143**, 034111 (2015).
[72]K. Pachucki, Phys. Rev. A **86**, 052514 (2012).
[73]M. Puchalski, J. Komasa, and K. Pachucki, Phys. Rev. A **95**, 052506 (2017).
[74]S. L. Bragg, J. W. Brault, and W. H. Smith, Astrophys. J. **263**, 999 (1982).
[75]A. Campargue, S. Kassi, K. Pachucki, and J. Komasa, Phys. Chem. Chem. Phys. **14**, 802 (2012).
[76]J. Komasa, K. Piszczatowski, G. Łach, M. Przybytek, B. Jeziorski, and K. Pachucki, J. Chem. Theory Comput. **7**, 3105 (2011).
[77]N. Chetty and V. W. Couling, J. Chem. Phys. **134**, 164307 (2011).
[78]G. Li, I. E. Gordon, L. S. Rothman, Y. Tan, S.-M. Hu, S. Kassi, A. Campargue, and E. S. Medvedev, Astrophys. J., Suppl. Ser. **216**, 15 (2015).
[79]D. Goorvitch, Astrophys. J., Suppl. Ser. **95**, 535 (1994).
[80]J. M. Huré and E. Roueff, Astron. Astrophys., Suppl. Ser. **117**, 561 (1996).
[81]C. Chackerian, Jr., R. Farrenq, G. Guelachvili, C. Rossetti, and W. Urban, Can. J. Phys. **62**, 1579 (1984).
[82]S. R. Langhoff and C. W. Bauschlicher, J. Chem. Phys. **102**, 5220 (1995).
[83]J. A. Coxon and P. G. Hajigeorgiou, J. Chem. Phys. **121**, 2992 (2004).
[84]S. Coriani, A. Halkier, D. Jonsson, J. Gauss, A. Rizzo, and O. Christiansen, J. Chem. Phys. **118**, 7329 (2003).
[85]W. L. Meerts, F. H. D. Leeuw, and A. Dymanus, Chem. Phys. **22**, 319 (1977).
[86]P. J. Mohr, D. B. Newell, and B. N. Taylor, Rev. Mod. Phys. **88**, 035009 (2016).
[87]C. Graham, D. A. Imrie, and R. E. Raab, Mol. Phys. **93**, 49 (1998).
[88]A. D. Buckingham, R. L. Disch, and D. A. Dunmur, J. Am. Chem. Soc. **90**, 3104 (1968).
[89]V. V. Meshkov, A. V. Stolyarov, A. Y. Ermilov, E. S. Medvedev, V. G. Ushakov, and I. E. Gordon, J. Quant. Spectrosc. Radiat. Transfer **217**, 262 (2018).
[90]E. S. Medvedev, V. V. Meshkov, A. V. Stolyarov, and I. E. Gordon, J. Chem. Phys. **143**, 154301 (2015).
[91]S. N. Yurchenko, A. F. Al-Refaie, and J. Tennyson, Astron. Astrophys. **614**, A131 (2018).
[92]J. M. Brown, J. T. Hougen, K.-P. Huber, J. W. C. Johns, I. Kopp, H. Lefebvre-Brion, A. J. Merer, D. A. Ramsay, J. Rostas, and R. N. Zare, J. Mol. Spectrosc. **55**, 500 (1975).
[93]R. Weiss, Phys. Rev. **131**, 659 (1963).
[94]F. H. de Leeuw and A. Dymanus, J. Mol. Spectrosc. **48**, 427 (1973).
[95]P. Piecuch, A. E. Kondo, V. Špirko, and J. Paldus, J. Chem. Phys. **104**, 4699 (1996).
[96]G. Maroulis, J. Mol. Struct.: THEOCHEM **633**, 177 (2003).
[97]J. F. Harrison, J. Chem. Phys. **128**, 114320 (2008).
[98]A. J. Sadlej, Collect. Czech. Chem. Commun. **53**, 1995 (1988).
[99]J. A. Coxon and P. G. Hajigeorgiou, J. Quant. Spectrosc. Radiat. Transfer **151**, 133 (2015).
[100]J. F. Noxon, Can. J. Phys. **39**, 1110 (1961).
[101]T. Földes, P. Čermák, M. Macko, P. Veis, and P. Macko, Chem. Phys. Lett. **467**, 233 (2009).
[102]E. H. Fink, H. Kruse, D. A. Ramsay, and M. Vervloet, Can. J. Phys. **64**, 242 (1986).
[103]H. J. Werner, P. J. Knowles, G. Knizia, F. R. Manby, M. Schütz, P. Celani, W. Györffy, D. Kats, T. Korona, R. Lindh, A. Mitrushenkov, G. Rauhut, K. R. Shamasundar, T. B. Adler, R. D. Amos, A. Bernhardsson, A. Berning, D. L. Cooper, M. J. O. Deegan, A. J. Dobbyn, F. Eckert, E. Goll, C. Hampel, A. Hesselmann, G. Hetzer, T. Hrenar, G. Jansen, C. Köppl, Y. Liu, A. W. Lloyd, R. A. Mata, A. J. May, S. J. McNicholas, W. Meyer, M. E. Mura, A. Nicklass, D. P. O'Neill, P. Palmieri, D. Peng, K. Pflüger, R. Pitzer, M. Reiher, T. Shiozaki, H. Stoll, A. J. Stone, R. Tarroni, T. Thorsteinsson, and M. Wang, MOLPRO, version 2015.1, a package of *ab initio* programs, 2015, see http://www.molpro.net.